Review Article

Survey of the Thermodynamic Properties of the Charge Density Wave Systems

M. Saint-Paul [iD][1,2] and P. Monceau[1,2]

[1] *Université Grenoble Alpes, Institut Néel, F-38042 Grenoble, France*
[2] *CNRS, Institut Néel, F-38042 Grenoble, France*

Correspondence should be addressed to M. Saint-Paul; michel.saint-paul@neel.cnrs.fr

We reexamine the thermodynamic properties such as specific heat, thermal expansion, and elastic constants at the charge density wave (CDW) phase transition in several one- and two-dimensional materials. The amplitude of the specific heat anomaly at the CDW phase transition T_{CDW} increases with increasing T_{CDW} and a tendency to a lineal temperature dependence is verified. The Ehrenfest mean field theory relationships are approximately satisfied by several compounds such as the rare earth tritelluride compound $TbTe_3$, transition metal dichalcogenide compound $2H\text{-}NbSe_2$, and quasi-one-dimensional conductor $K_{0.3}MoO_3$. In contrast inconsistency exists in the Ehrenfest relationships with the transition metal dichalcogenide compounds $2H\text{-}TaSe_2$ and $TiSe_2$ having a different thermodynamic behavior at the transition temperature T_{CDW}. It seems that elastic properties in the ordered phase of most of the compounds are related to the temperature dependence of the order parameter which follows a BCS behavior.

1. Introduction

The electron density of a low dimensional (one-dimensional (1D) or two-dimensional (2D)) compound may develop a wavelike periodic variation, a charge density wave (CDW), accompanied by a lattice distortion when temperature drops below a critical temperature T_{CDW} [1–46]. CDW ordering is driven by an electron phonon coupling. The concept of charge density wave is related to the initial work of Peierls [1], followed by Fröhlich [2] when it was demonstrated that a one-dimensional metal is instable with respect to a phase transition in the presence of electron phonon coupling.

A charge density wave is characterized by a spatial periodic modulation of the electronic density concomitant with a lattice distortion having the same periodicity. The properties of the CDW state can be described by an order parameter $Q \exp(i\Phi)$ [1]. The fluctuations of the lattice distortions can be described by amplitude and phase modes [1]. This variation, charge density wave, in the electron density is receiving intense study because it often competes with another ground state (superconductivity). A CDW order can be formed with one fixed wave vector or multiple wave vectors. For example, the incommensurate ordering vector Q_1 of the prototypal rare earth tritelluride $ErTe_3$ at the upper CDW phase transition T_{CDW1} = 265 K is parallel to the $\vec{c}$ axis, whereas the incommensurate ordering parameter Q_2 observed at the lower CDW phase transition T_{CDW2} = 150 K with $ErTe_3$ is parallel to the $\vec{a}$ axis. In contrast the CDW order in the dichalcogenide compounds (for example, $2H\text{-}NbSe_2$) is formed by three superposed charge density waves.

The origin of the CDW phase transition observed in the two-dimensional materials is still not completely settled [5]. Two alternatives have been proposed for describing the nature of the CDW in the family of rare earth tritelluride RTe_3 (R=rare earth element) which represents a charge density model. Based on ARPES measurements [10, 11], one describes it in terms of Fermi surface nesting following the electron Peierls scheme. The other one emphasizes the role of the strongly momentum dependent electron phonon coupling as evidenced from inelastic X-ray scattering [13] and Raman [7, 14] experiments. As the electron phonon coupling is increased the importance of the electronic structure in k space is reduced.

Study of the thermodynamic properties of the charge density wave phase transition in two-dimensional transition metal dichalcogenide compounds [16–25] and in quasi-one-dimensional conductors [26–37] has generated a considerable interest over the past 30 years. The onset of the CDW order has remarkable effects on the thermodynamic properties since below T_{CDW} a gap opens up in the density of the electronic states. A microscopic model is given by McMillan [28]. The elastic properties of quasi low dimensional conductors undergoing charge and spin density phase transitions are reviewed by Brill [3]. Several reviews discuss the properties of the charge density wave systems [4–6, 45].

We reexamine the thermodynamic experimental data such as specific heat, thermal expansion, and elastic constants of several CDW compounds. We give a survey of the Ehrenfest relations using the experimental data obtained at the CDW phase transition in different materials: rare earth tritellurides RTe$_3$ (TbTe$_3$, ErTe$_3$, and HoTe$_3$) [8, 41–43], transition metal dichalcogenides MX$_2$ compounds (2H-NbSe$_2$ [17–19], 2H-TaSe$_2$ and 2H-TaS$_2$ [16, 24, 25], and TiSe$_2$ [20–23]), quasi-one-dimensional conductors (NbSe$_3$ [25, 27], K$_{0.3}$MoO$_3$ [30–33], (TaSe$_4$)$_2$I [39, 40], and TTF-TCNQ [35–38]), and in the system (LaAgSb$_2$) [44, 45].

Departures from the mean field behavior of the thermodynamic properties are generally attributed to fluctuations which belong to the 3D XY criticality class [27–34]. The contribution of the fluctuations is important in the quasi-one-dimensional conductors [28] and in the transition metal dichalcogenides (2H-TaSe$_2$, 2H-TaS$_2$) [24]. Small fluctuation effects are observed around T_{CDW} in the rare earth tritellurides TbTe$_3$ [41] and ErTe$_3$ [42].

The amplitude of the lattice distortion is governed by the electron phonon coupling strength [46]. A moderately strong electron phonon coupling is reported for the rare earth tritellurides (ARPES experiments [10, 11]), similar to that observed in quasi-1D CDW systems such as K$_{0.3}$MoO$_3$ and NbSe$_3$. In a weak coupling CDW, the specific heat behavior at the CDW phase transition is driven by the electronic entropy [28, 46]. In a strong coupling CDW the transition is also governed by the entropy of the lattice [28, 46].

2. Thermodynamic Properties

2.1. Ehrenfest Relations.
At a second-order phase transition T_C, the order parameter Q increases continuously in the ordered phase at T $<$ T$_C$. The Landau free energy [47] can be written without knowing the microscopic states as

$$F = F_0 + a\left(T - T_C\right)Q^2 + BQ^4, \tag{1}$$

where F_0 describes the temperature dependence of the high temperature phase and the constant parameters a and B are positive. The order parameter that minimizes the free energy ($\partial F/\partial Q = 0$) is given by

$$Q^2 = \frac{aT_{CDW}}{2B}\left(1 - \frac{T}{T_{CDW}}\right). \tag{2}$$

The entropy (S) is derived from the free energy (F), $S = -\partial F/\partial T$, and the specific heat at constant pressure is given

by $C_P = T[\partial S/\partial T]_P$. There is a jump in the specific heat (Figure 1(a)) at the second-order phase transition T_C given by [47]

$$\Delta C_P = \frac{a^2 T_C}{2B}. \tag{3}$$

Discontinuities in the thermal expansion coefficients and the elastic constants are also observed at a second-order phase transition. An example (TbTe$_3$) is shown in Figures 1(b) and 1(c). The thermodynamic quantities at a second-order phase transition such as a charge density wave phase transition are generally discussed with the Ehrenfest relations reformulated by Testardi [48]. The discontinuity in the thermal expansion coefficients α_i is related to the specific heat jump ΔC_P and to the stress dependence components, $\partial T_{CDW}/\partial\sigma_i$, at the phase transition T_{CDW}:

$$\Delta\alpha_i = -\frac{\Delta C_P}{V_m T_{CDW}}\frac{\partial T_{CDW}}{\partial\sigma_i}, \tag{4}$$

where i=1, 2, and 3 correspond to the $\vec{a}$, $\vec{b}$, and $\vec{c}$ crystallographic axes directions and V_m is the molar volume.

The elastic constant component C_{ii} is related to the elastic velocity V_{ii} by $C_{ii} = \rho V_{ii}^2$, ρ being the mass density. The discontinuities of the elastic constants $\Delta C_{ii}/C_{ii}$ (or velocity $\Delta V_{ii}/V_{ii} = \Delta C_{ii}/2C_{ii}$) at a second-order phase transition are related to the stress dependence $\partial T_{CDW}/\partial\sigma_i$ by

$$\frac{\Delta V_{ii}}{V_{ii}} = -\frac{\rho V_{ii}^2 \Delta C_P}{2V_m T_{CDW}}\left[\frac{\partial T_{CDW}}{\partial\sigma_i}\right]^2. \tag{5}$$

The term, $\rho V_{ii}^2 \Delta S(\partial^2 T_{CDW}/\partial\sigma_i^2)$, proportional to the entropy variation and multiplied by the second derivative $\partial^2 T_{CDW}/\partial\sigma_i^2$ [3, 31], is neglected in (5). Isothermal elastic constants must be used in (5). But the adiabatic elastic constants are measured in the MHz range and the adiabatic values are generally used in (5).

From (4) and (5)

$$\frac{\Delta V_{ii}}{V_{ii}} = -\frac{\rho V_{ii}^2 V_m T_{CDW}}{2\Delta C_P}\left[\Delta\alpha_i\right]^2. \tag{6}$$

Thus the discontinuities in the elastic velocities are proportional to the square of the discontinuities in the expansion coefficients. Typical discontinuities of the specific heat, thermal expansion coefficient, and elastic velocity at the charge density wave transition are shown in Figure 1. The discontinuities of the elastic constants at T_{CDW} are evaluated using the extrapolated linear temperature dependence of the high temperature background as shown in Figures 1(a) and 1(b).

2.2. Elastic Constants.
CDW materials acquire lattice distortions that are incommensurate with the basic lattice. They form part of a wider field of interest developed in the incommensurate structures [49, 50]. Incommensurate structures may arise with insulators as K$_2$SeO$_4$ [51]. The structural changes are characterized by a distortion whose wave vector
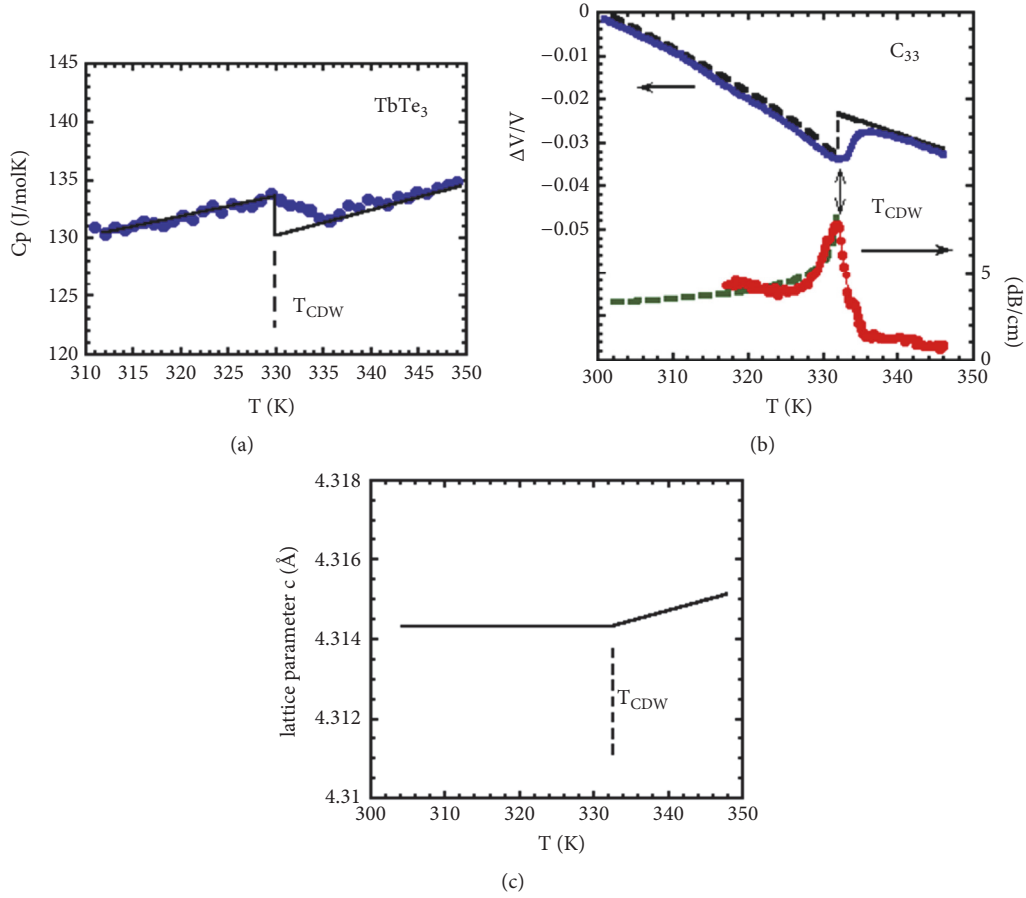
FIGURE 1: *Color on line*. Temperature dependence of the thermodynamic properties of TbTe$_3$. (a) Specific heat measurements taken from [41]. (b) Relative change of the velocity (blue), ultrasonic attenuation (red), and fit (dashed black curve) taken from [41]. (c) The lattice parameter c measured by X-rays taken from [8].

cannot be expressed by a rational fraction of the lattice vector. The resulting ordered phase is not strictly crystalline and is described by an incommensurate phase.

The amplitude of the modulation increases continuously as the temperature is lowered. The relationship between the crystalline and the modulated phases can be formulated in the framework of the Landau theory [28]. In some materials, as 2H-TaSe$_2$, the modulation periodicity is temperature dependent and may be lock-in at low temperatures to a value that is commensurate with the periodicity of the basis structure [28, 46]. The lock-in transition is a first-order phase transition and very different in nature from the incommensurate instability [46]. 2H-TaSe$_2$ undergoes a normal to incommensurate transition (second-order) at 122 K and an incommensurate-commensurate transition (first-order) at 90 K [16]. The transition to the incommensurate structural phase is reflected in the elastic stiffness components analyzed in [51, 52].

In order to explain the stiffening of the elastic constants (velocities) in the ordered phase below the incommensurate structural phase transition, a first approach based on the

analysis of the entropy variation around the CDW phase transition T_{CDW} is proposed in [3]. A second approach was developed by Rhewald [51] based on the Landau phenomenological theory including the interaction between the strain components e_i and the square of the order parameter Q [51, 52]. The expansion of the free energy density in power of Q^2 and e_i is developed in agreement with the symmetry point group of the material [51, 52].

In the orthorhombic symmetry, for example, the free interaction energy is given by

$$F_c\left(e_i, Q\right) = \left[g_1 e_1 + g_2 e_2 + g_3 e_3\right] Q^2$$
$$+ \frac{1}{2}\left[\sum_{i,j}^{3} h_{ij} e_i e_j + \sum_{i=4}^{6} h_{ii} e_i^2\right] Q^2, \quad (7)$$

where g and h are the coupling constants.

The interacting terms linear in e_i and quadratic in Q as $g_i e_i Q^2$ are responsible for a decrease of the longitudinal elastic constant C_{ii} (velocity V_{ii}). The decrease of the longitudinal

elastic constant C_{ii} is proportional to the square of the coupling constant g_i:

$$\Delta C_{11} \sim -g_i^2$$

$$\Delta C_{22} \sim -g_2^2 \quad\quad (8)$$

$$\Delta C_{33} \sim -g_3^2.$$

The coupling second terms $e_i^2 Q_2$ in (7) show that several elastic constants C_{ij} (or velocities) follow the temperature dependence of the square of the static value of the order parameter $\langle Q \rangle$ in the ordered phase below T_{CDW} [51, 52]:

$$\Delta C_{ij} \sim h_{ij} \langle Q \rangle^2 \quad \text{for ij} = 11, 22, 33, 44, 55, 66. \quad (9)$$

The temperature dependence of the sound velocity and the amplitude of the superlattice reflections gives directly the temperature dependence of the order parameter [1].

This general behavior has been observed at the CDW phase transition T_{CDW} in different materials [16, 17, 20, 36, 37, 41–43]. The hardening observed in the ordered phase with several compounds is analyzed in Section 3.5.

3. Results

3.1. Specific Heat Anomaly at the CDW Phase Transition. We reexamine the specific heat discontinuities ΔC_P measured at the CDW phase transitions in the following materials:

(a) Rare earth tritellurides TbTe$_3$ [41] and ErTe$_3$ [42]

(b) Transition metal dichalcogenides 2H-NbSe$_2$ [19], TiSe$_2$ [22, 23], 2H-TaSe$_2$, and 2H -TaS$_2$ [24]: The mean field contribution for 2H-TaSe$_2$ and 2H-TaS$_2$ was estimated in [23]. These two compounds are characterized by large fluctuations

(c) Quasi-one-dimensional conductors NbSe$_3$ [26], K$_{0.3}$MoO$_3$ [30, 31], (TaSe$_4$)$_2$I [40], and TTF-TCNQ [35]

(d) Three-dimensional material LaAgSb$_2$ [44] and Cr [53]

The specific heat discontinuities ΔC_P are reported in Tables 1–4 and they are shown as a function of the CDW phase transition temperature T_{CDW} in Figure 2. A linear dependence is expected $\Delta C_P = A T_{CDW}$. The experimental data are situated inside the area determined by the two linear dependence types (1) and (2) (Figure 2). The first line (1) followed by TTF-TCNQ, 2H-TaS$_2$, and 2H-TaSe$_2$ has a larger coefficient $A_1 = 4 \times 10^{-2}$ J/molK^{-2}. The second line (2) has a coefficient $A_2 = 3 \times 10^{-3}$ J/molK^{-2}, 10 times smaller than A_1. This second line is followed approximately by the rare earth tritelluride compounds ErTe$_3$ and TbTe$_3$ at the upper and lower CDW phase transitions (blue circle and black circles). The specific heat discontinuity found at the upper CDW phase transition with LaAgSb$_2$ (red square symbol) is also situated on line (2).

However it should be noted that substantial differences exist between the experimental specific heat results obtained from different groups.
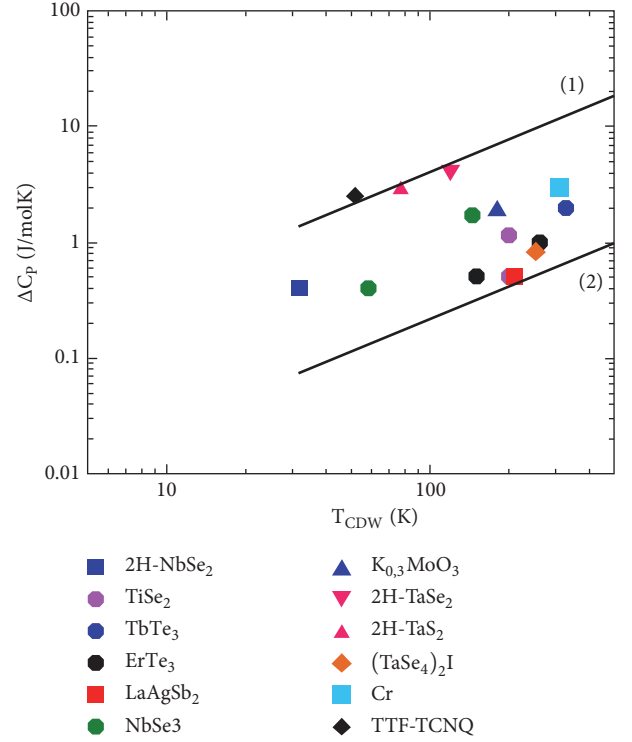

FIGURE 2: *Color on line.* Heat specific discontinuities ΔC_P at the CDW phase transition T_{CDW} (Table 1) as a function of T_{CDW}. TbTe$_3$ (blue circle) [41]; ErTe$_3$ (black circles $T_{CDW1} = 260$ K, $T_{CDW2} = 155$ K) [42]; TiSe$_2$ (violet circles, $T_{CDW} = 200$ K with two different results given in [22, 23]); LaAgSb$_2$ (red square $T_{CDW1} = 210$ K) [44]; NbSe$_3$ (green circle $T_{CDW1} = 145$ K, $T_{CDW2} = 48$ K) [26]; 2H-NbSe$_2$ (blue squares $T_{CDW} = 30$ K) [19]; 2H-TaSe$_2$ (red down triangle T_{CDW} $= 120$ K) and 2H-TaS$_2$ (red up triangles $T_{CDW} = 80$ K) mean field contribution given by [24]; TTF-TCNQ (black diamond symbol mean field contribution given in [35]); K$_{0.3}$MoO$_3$ (blue up triangles $T_{CDW} = 180$ K) two different results given by [30]; (TaSe$_4$)$_2$I (brown diamond $T_{CDW} = 260$ K [40]); Cr (light blue square [53]). Lines (1) and (2) are lineal temperature dependence.

3.2. Thermal Expansion Anomaly at the CDW Phase Transition. Anisotropic anomalies of the elastic velocities and thermal expansion coefficients are observed at the CDW phase transition of the compounds under review.

(a) Discontinuities $\Delta\alpha$ of the thermal expansion coefficient in the basal plane at the upper phase transition $T_{CDW1} = 330$ K of TbTe$_3$ were obtained from thermal expansion measurements using X-rays technique by Ru et al. [8]. At the upper phase transition, the incommensurate wave vector is along the $\vec{a}$ axis. Large anisotropic behavior is observed for the thermal expansion along the $\vec{c}$ and $\vec{a}$ axes. The largest discontinuity is observed along the $\vec{c}$ axis [8] and is only reported in Table 1.

The discontinuities $\Delta\alpha$ along the $\vec{a}$ and $\vec{c}$ axes at the lower CDW phase transition $T_{CDW2} = 150$ K of ErTe$_3$ were obtained from the thermal expansion measurements using X-rays technique by Ru [8].

TABLE 1: Materials (2D CDW) TbTe$_3$, HoTe$_3$, and ErTe$_3$ rare earth tritellurides. Molar volumes are given in cm^3, specific heat discontinuities in J/molK, thermal expansion discontinuities in K^{-1}, elastic velocity discontinuities in $\Delta V/V$, and measured and calculated elastic constants in GPa and ratios.

Materials	Molar volume cm^3	T_{CDW} K	Specific heat ΔC_p J/molK	Thermal expansion coefficient along the $\overrightarrow{c}$ axis $\Delta\alpha_c$ (K^{-1})	Elastic velocity decrease $\Delta V/V$	Elastic constant Measured GPa	calculated ρV^2 GPa	Ratio Calculated /measured
TbTe$_3$	71	330	3 [41]	-1.2x10^{-5} [8]	along the $\overrightarrow{a}$ or $\overrightarrow{c}$ axis -0.01 [41]	C$_{33}$ ~ 50	25	~0.5
HoTe$_3$	70.4	280 120			Along the $\overrightarrow{c}$ axis -0.025 [43] -0.001	C$_{33}$ ~ 50		
ErTe$_3$	69.7	260 150	1 [42] 0.5	-3.5x10^{-6} [8]	along the $\overrightarrow{a}$ or $\overrightarrow{c}$ axis -0.015 [42] -0.001	C$_{33}$ ~ 50	20	~0.4

TABLE 2: Materials (2D CDW) transition metal dichalcogenides 2H-NbSe$_2$, TiSe$_2$, 2H-TaSe$_2$, and 2H-TaS$_2$. Molar volumes are given in cm^3, specific heat discontinuities in J/molK, thermal expansion discontinuities in K^{-1}, elastic velocity discontinuities in $\Delta V/V$, and measured and calculated elastic constants in GPa. Discrepancies exist among the experimental values of the Young modulus; the largest values are only indicated. Ratio = calculated ρV^2/experimental elastic constant.

Materials	Molar volume cm^3	T_{CDW} K	Specific heat ΔC_p J/molK	Thermal expansion coefficient $\Delta\alpha$ K^{-1}	Elastic velocity decrease $\Delta V/V$	Elastic constant GPa	calculated ρV^2 GPa	Ratio
2H-NbSe$_2$	40	30	0.5 [19]	$\overrightarrow{c}$ axis -3×10^{-6} [19] $\overrightarrow{c}$ axis -2×10^{-7} [18]	$\overrightarrow{a}$ axis -5×10^{-4} [16, 17]	C_{11}=108 [17] C_{33}=460	35	~0.3
TiSe$_2$	39.6	200	1.15 [22] 0.5 [23]	$\overrightarrow{a}$ axis -2.5×10^{-6} [19]	along the $\overrightarrow{a}$ axis -0.05 [19]	$\overrightarrow{a}$ axis $C_{11}\sim190$ [20]	1800 800	~10 ~4
2H-TaSe$_2$		120	4 [24]	$\overrightarrow{a}$ axis -8×10^{-6} [25]	$\overrightarrow{a}$ axis -0.0005 [16, 17]	Young modulus ($\overrightarrow{a}$ axis) $E_a\sim120$ [16]	16	~0.1
2H-TaS$_2$	35.7	78	2.8 [24]		no discountin.			

TABLE 3: Materials (1D CDW), quasi-one-dimensional conductors $K_{0.3}MoO_3$, $NbSe_3$, $(TaSe_4)_2I$, and TTF-TCNQ. Molar volumes are given in cm³, specific heat discontinuities in J/molK, thermal expansion discontinuities in K⁻¹, elastic velocity discontinuities in $\Delta V/V$, and measured and calculated elastic constants in GPa and ratios.

Materials	Molar volume cm³	T_{CDW} (K)	Specific heat ΔC_p J/molK	Thermal expansion coefficient $\Delta\alpha$ (K⁻¹)	Elastic velocity decrease $\Delta V/V$	Elastic constant GPa	calculated ρV^2 GPa	Ratio calculated /measured
$K_{0.3}MoO_3$	36.3	180	3.6 [30] 2 [34]	[102] axis 7×10^{-6} [31]	[102] axis -0.02 [31]	[102] axis Young modulus 250 [31] 60 [33]	250 [31]	~1 ~4
$(TaSe_4)_2I$	180	260	0.83 [40]	$\overrightarrow{c}$ axis -1×10^{-6} [38]	$\overrightarrow{c}$ axis -0.001 [37]	$C_{33}=115$ [37]	37	~0.3
$NbSe_3$	40.8	145 58	3 [26] 0.4 [26]	in plane -2×10^{-6} [25]	-0.0003 [27]	550 [27]	70	~0.1
TTF-TCNQ	250	55	2.5 [35]	No discontinuity [36]	$\overrightarrow{c}$ axis -0.01 [37] ~0 [36]	Young modulus E~60 [37] E~15 [36]		

TABLE 4: Three-dimensional materials. Molar volumes are given in cm^3, specific heat discontinuities in J/molK, thermal expansion discontinuities in K^{-1}, elastic velocity discontinuities in $\Delta V/V$, and measured and calculated elastic constants in GPa and ratios.

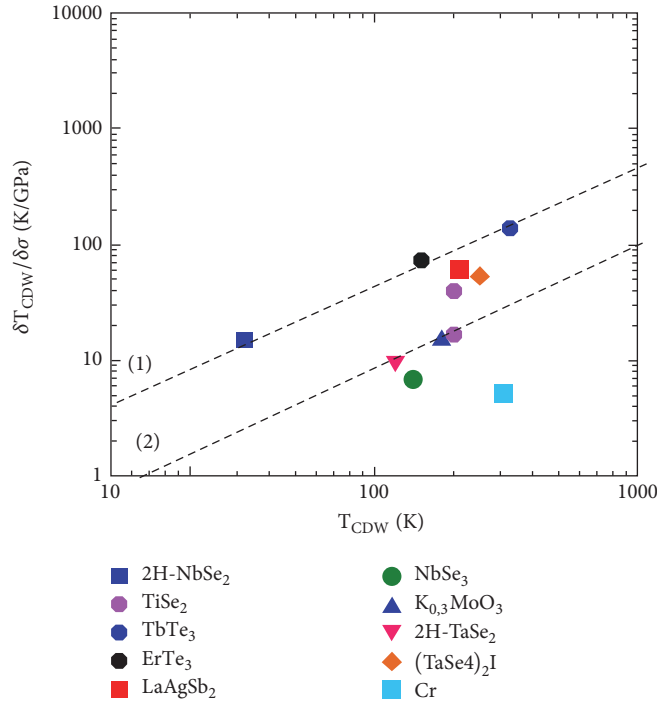| Materials	Molar volume cm^3	T_{CDW}, T_N K	Specific heat J/molK	Thermal expansion coefficient $\Delta\alpha$ K^{-1}	Elastic velocity decrease	Elastic Constant GPa	calculated ρV^2 GPa	Ratio calculated /measured
LaAgSb2	62.8	$T_{CDW1}=210$ $T_{CDW2}=185$	0.5 [44] 0.1 [44]	$\vec{c}$ axis 2.2x10^{-6} -5x10^{-7} [44]	No measurement			
Cr	7.2	$T_N=310$	3 [53]	along [100] -7x10^{-6} [54]	along [100] -0.03 [54]	$C_{11}=400GPa$ [54]	770	~2

FIGURE 3: *Color on line.* Stress dependence $\partial T_{CDW}/\partial \sigma$ derived from Ehrenfest eq. (4) with the thermal expansion coefficient discontinuities $\Delta\alpha$ (Tables 1 and 2) measured at the CDW phase transitions as a function of T_{CDW}. $\Delta\alpha$ along the $\vec{c}$ axis in TbTe$_3$ at T_{CDW1} = 330 K (blue circle) and ErTe$_3$ at T_{CDW2} = 150 K (black circle) deduced from the thermal expansion measurements using X-rays technique reported by Ru et al. [8]. Results with TiSe$_2$ (violet circle) T_{CDW} = 200 K [20]; 2H-TaSe$_2$ (pink down triangle) [25]; NbSe$_3$ (green circle T_{CDW} = 145 K) [25]; 2H-NbSe$_2$ (blue square) [18, 19]; K$_{0.3}$MoO$_3$ (blue up triangle T_{CDW} = 180 K) [31, 32]; (TaSe$_4$)$_2$I (brown diamond) [39]; LaAgSb$_2$ (red square T_{CDW1} = 210 K) [44]; and Cr (light blue square [54]). Lines (1) and (2) are lineal temperature dependence.

Similar discontinuities are observed along the $\vec{a}$ and $\vec{c}$ axes.

Only the values of $\Delta\alpha$ along the $\vec{c}$ axis are reported in Table 1.

(b) Thermal expansion coefficients discontinuities in the basal plane along the $\vec{a}$ and $\vec{c}$ axes obtained at the CDW transitions on transition metal dichalcogenides 2H-NbSe$_2$ [18, 19], TiSe$_2$ [20], and 2H-TaSe$_2$ [25] are reported in Table 2. Very different experimental results were found for 2H-NbSe$_2$ [18, 19].

(c) Thermal expansion discontinuities $\Delta\alpha$ determined along the [102] directions in NbSe$_3$ [25], K$_{0.3}$MoO$_3$ [31, 32], (TaSe$_4$)$_2$I [39], and TTF-TCNQ [38] are reported in Table 3.

(d) Finally the thermal expansion discontinuities along the $\vec{c}$ axis observed in LaAgSb$_2$ at the upper (T_{CDW1}= 210 K) and lower CDW phase transition (T_{CDW2} = 185 K) [44] are reported in Table 4. Thermal expansion discontinuity along the $\vec{a}$ axis observed at the spin density wave transition T_{SDW} = 310 K for chromium [54] is also reported in Table 4.

The stress dependence deduced using (4) from the thermal expansion coefficient discontinuities $\Delta\alpha$ measured at T_{CDW} along one crystallographic direction is given by

$$\frac{\partial T_{CDW}}{\partial \sigma} = -\Delta\alpha V_m \frac{T_{CDW}}{\Delta C_p}. \tag{10}$$

The stress dependence $\partial T_{CDW}/\partial \sigma$ values deduced at T_{CDW} from the values given in Tables 1–4 are reported versus the transition temperature T_{CDW} in Figure 3. It seems that $\partial T_{CDW}/\partial \sigma$ increases with increasing T_{CDW}. The high values of the stress dependence $\partial T_{CDW}/\partial \sigma$ are found with the rare earth tritellurides and 2H-NbSe$_2$. Such a high value $\partial T_{CDW}/\partial \sigma \sim$ 100 K/GPa obtained for TbTe$_3$ is in agreement with the value dT$_{CDW}$/dp = 85K/GPa obtained in the hydrostatic measurements [15]. Smaller (one order of magnitude smaller) values of the stress dependence $\partial T_{CDW}/\partial \sigma$ are found with the transition metal dichalcogenide compounds and the quasi-one-dimensional conductors.

It results in the fact that a high lattice anharmonicity is responsible for such a large stress dependence of T$_{CDW}$ observed in the rare earth tritelluride materials.

3.3. Elastic Constant (Velocity) Anomaly at the CDW Phase Transition. The steplike decrease of the longitudinal elastic
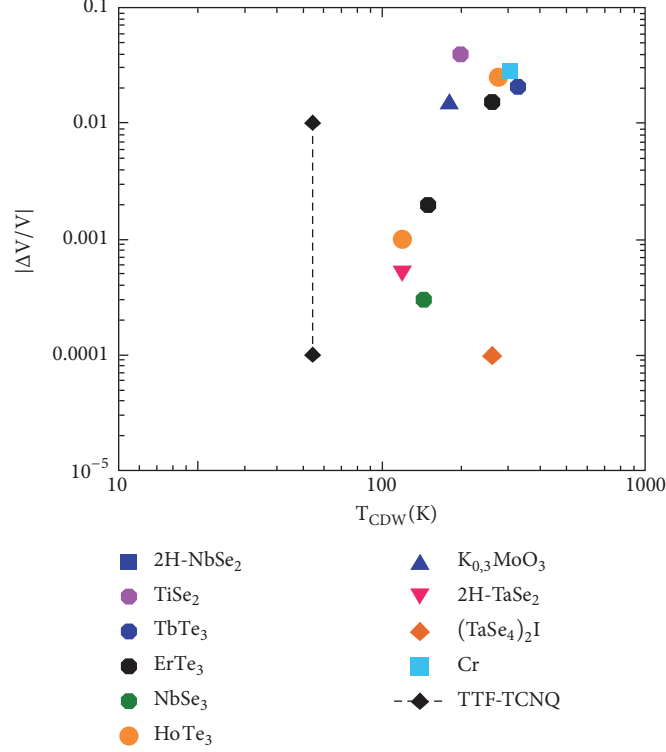
FIGURE 4: *Color on line*. Experimental discontinuities (absolute values) $|\Delta V/V|$ of the velocity of the longitudinal C_{11} and C_{33} shown as a function of T_{CDW} (Tables 1 and 2). Results obtained with $TbTe_3$ (blue circle T_{CDW} = 330 K) [41], $ErTe_3$ (black circles T_{CDW1} = 260 K and T_{CDW2} = 155 K) [42], and $HoTe_3$ (brown circles T_{CDW1} = 280 K and T_{CDW2} = 120 K) [43]. Results obtained by Young and velocity measurements $NbSe_3$ (green circle) [27], $2H$-$NbSe_2$ (blue squares) [16, 17], $TiSe_2$ (violet circle) [20], $2H$-$TaSe_2$ (red down triangle) [16], $K_{0.3}MoO_3$ (blue up triangle [31]), $(TaSe_4)_2I$ (brown diamond) [39], TTF-TCNQ (black diamonds) with a large discrepancy (~0.0001, 0.01 shown by the dotted black line [36, 37]), and Cr (light blue [54]).

velocity $\Delta V_{33}/V_{33} = \Delta C_{33}/2C_{33}$ along the $\overrightarrow{c}$ axis measured at the upper and lower CDW phase transitions in the rare earth tritelluride $TbTe_3$ [41], $ErTe_3$ [42], and $HoTe_3$ [43] compounds is reported in Table 1.

The sound velocity and the Young modulus E discontinuities (velocity discontinuity deduced from E is given by $\Delta V/V = \Delta E/2E$) were measured in the a-b plane at the CDW phase transition in dichalcogenides $2H$-$NbSe_2$ [16, 17], $TiSe_2$ [20], $2H$-$TaSe_2$ [16, 17], and $2H$-TaS_2 [16, 17], in quasi-one-dimensional conductors $K_{0.3}MoO_3$ [31, 33] and $(TaSe_4)_2I$ [39] (Tables 2 and 3).

Two different values $\Delta V/V \sim 0$ and ~0.01 (dotted black line in Figure 4) are reported for the organic conductor TTF-TCNQ [36, 37]. The discontinuity measured at the SDW phase transition (T_N = 310 K) of Chromium [54] is also reported in Table 4. All the absolute values $\Delta V/V$ are shown in Figure 4.

Very small values are reported for $2H$-$TaSe_4$ and $(TaSe_4)_2I$. A general tendency is observed: the amplitude of the sound velocity discontinuities increases with T_{CDW}. We mention that large discrepancies exist among the experimental Young modulus values.

3.4. Consistency. The consistency of Ehrenfest relations (1) and (2) may be checked by evaluating the value ρV^2, equivalent to an effective elastic constant, from the discontinuities

$\Delta V/V$, $\Delta\alpha$, and ΔC_p measured at the CDW phase transition from different experiments following (6) which is rewritten as

$$[\rho V^2]_{calcultaed} = 2\frac{1}{V_m\,(\Delta\alpha)^2}\left[-\frac{\Delta V}{V}\right]\frac{\Delta C_P}{T_{CDW}} \qquad (11)$$

The values $C_{calculated} = \rho V^2$ evaluated using (11) with different materials are indicated in Tables 1–4.

A realistic value of about 20 GPa is found for the rare earth tritelluride compounds $TbTe_3$ and $ErTe_3$. An unrealistic value of about 5000 GPa is evaluated with the very small thermal expansion jump value, $\Delta\alpha \sim 2 \times 10^{-7}$ K^{-1}, measured with $2H$-$NbSe_2$ in [18]. In contrast the thermal expansion results, $\Delta\alpha \sim 3 \times 10^{-6}$ K^{-1}, reported in [19] give a value ~35 GPa. A realistic value 250 GPa is evaluated for $K_{0.3}MoO_3$ in [31]. A smaller value of 37 GPa is obtained for the one-dimensional conductor $(TaSe_4)_2I$. In contrast large values 1800 GPa and 800 GPa are obtained for $TiSe_2$. A small value of about 16 GPa is evaluated for $2H$-$TaSe_2$. No discontinuity, $\Delta\alpha \sim 0$, is observed for TTF-TCNQ and $C_{calculated}$ given by (11) cannot be evaluated for this material (Table 3). Finally a realistic value $C_{calculated}$ is evaluated (see (11)) at the SDW phase transition in chromium which has been previously discussed in [53–55]. The ratio values between $C_{calculated}$ and the measured elastic constant are shown in Figure 5.
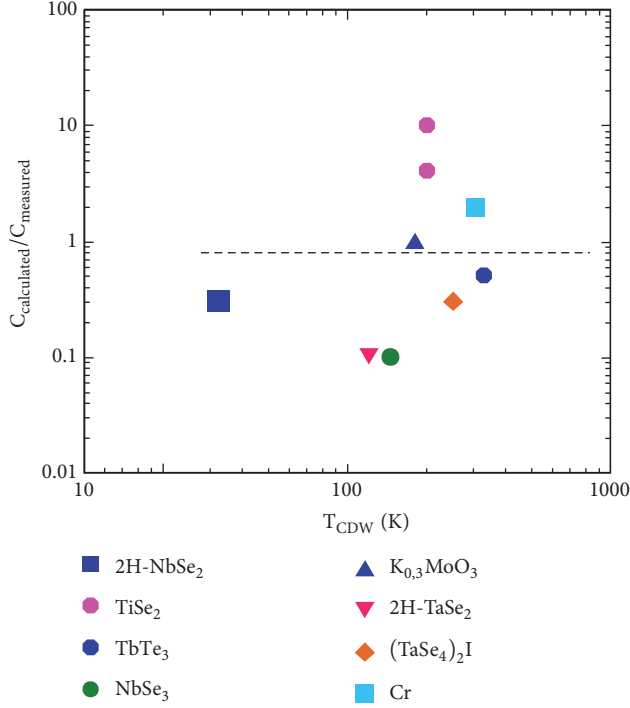
FIGURE 5: *Color on line*. Ratio between the calculated elastic constants ($C_{calculated}$) using (11) and the measured values of the elastic constants (Tables 1–4), $C_{calculated}/C_{measured}$ (column 10 in Tables 1–4). $C_{calculated}/C_{measured} \sim 1$ indicates that the Ehrenfest relations are satisfied.

In conclusion the Ehrenfest equations are approximately satisfied by several materials: the rare earth tritellurides $TbTe_3$ and $ErTe_3$, the transition metal dichalcogenide 2H-$NbSe_2$, and the one-dimensional conductors $K_{0.3}MoO_3$ and $(TaSe_4)_2I$. In the same manner the Ehrenfest equations are quantitatively satisfied at the SDW phase transition temperature (Néel antiferromagnetic phase transition) in chromium as discussed in [55]. In contrast the metal transition dichalcogenide 2H-$TaSe_2$ and $TiSe_2$ compound do not satisfy the Ehrenfest equations.

3.5. Temperature Dependence of the CDW Order Parameter.
The increase of the elastic velocity ΔV below T_{CDW} shown by the dotted black line in Figure 1(b) is related to the square of the order parameter $Q(T)$ (see (9)). $\Delta V/V$ is analyzed with the following relation:

$$\frac{\Delta V}{V} = \left[\frac{\Delta V}{V}\right]_0 \left(\frac{Q(T)}{Q(0)}\right)^2 \qquad (12)$$

where $Q(0)$ is the value of the order parameter at T= 0K and $[\Delta V/V]_0$ is the maximum value of the relative velocity at T=0K and $\Delta V/V = 0$ at T_{CDW}. For simplicity all the data are normalized at T=0 where $\Delta V/V = 0$. It results in the fact that (12) is changed by

$$\frac{\Delta V}{V} = \left[\frac{\Delta V}{V}\right]_0 \left\{\left[\frac{Q(T)}{Q(0)}\right]^2 - 1\right\}. \qquad (13)$$
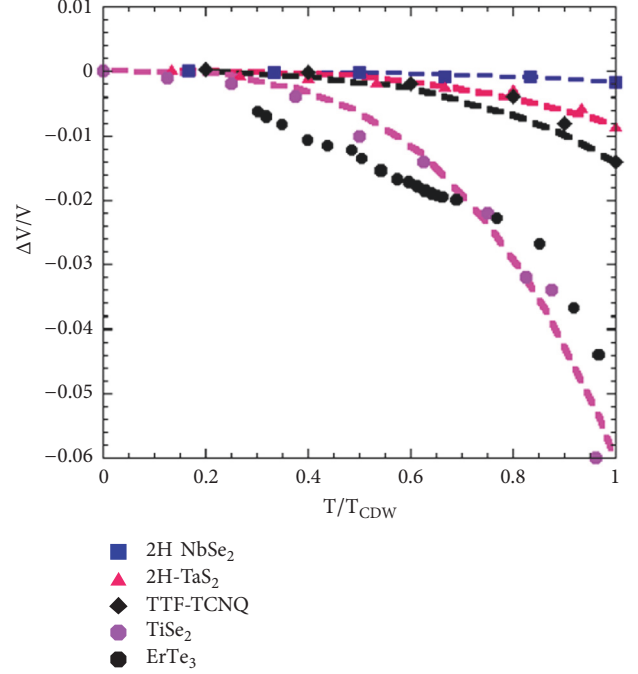

FIGURE 6: *Color on line*. Temperature dependence of the measured relative velocity $\Delta V/V$ as a function of the reduced temperature T/T_{CDW}. Velocity of the longitudinal mode in the *(a b)* plane in $TiSe_2$ [20], 2H-TaS_2 [16, 17], 2H-$NbSe_2$ [16, 17], and TTF-TCNQ [36]. Velocity of the mode C_{33} measured with $ErTe_3$ at the upper CDW phase transition $T_{CDW} = 260$ K [42]. The dashed curves are calculated with the BCS theory (see (14)).

The temperature dependence of the velocity $\Delta V/V$ of the longitudinal modes measured in the different materials is reported in Figure 6. All the experimental data follow the temperature dependence of the square of the BCS order parameter $[Q(T)/Q(0)]^2_{BCS}$ [1]:

$$\frac{\Delta V}{V} = \left[\frac{\Delta V}{V}\right]_0 \left\{\left[\frac{Q(T)}{Q(0)}\right]^2_{BCS} - 1\right\}. \qquad (14)$$

The blue dashed curve is calculated with $0.0017\{[Q(T)/Q(0)]^2_{BCS} - 1]\}$ for 2H-$NbSe_2$ with $T_{CDW} = 32$ K [16, 17]. The pink dashed curve is calculated with $0.0086\{[Q(T)/Q(0)]^2_{BCS} - 1\}$ for 2H-TaS_2 with $T_{CDW}=75$ K [16, 17]. The black dashed curve is calculated with $0.014\{[Q(T)/Q(0)]^2_{BCS} - 1\}$ for TTF-TCNQ with $T_{CDW} = 50$ K [36] and the violet dashed curve with $0.06\{[Q(T)/Q(0)]^2_{BCS} - 1\}$ for $TiSe_2$ with $T_{CDW} = 200$ K [20]. The black circles are values for $ErTe_3$ with $T_{CDW} = 260$ K [42].

A remarkable feature is the increase of the amplitude $[\Delta V/V]_0$ with T^2_{CDW}, $[\Delta V/V]_0 \sim 10^{-6} \times T^2_{CDW}$, in Figure 7. It yields the fact that the order parameter $Q(0)$ proportional to $\{[\Delta V/V]_0\}^{0.5}$ increases with the charge density wave transition temperature T_{CDW} in agreement with BCS theory.

In conclusion the temperature dependence of the elastic velocity is compatible with the BCS behavior in agreement with the temperature dependence of the amplitude of the
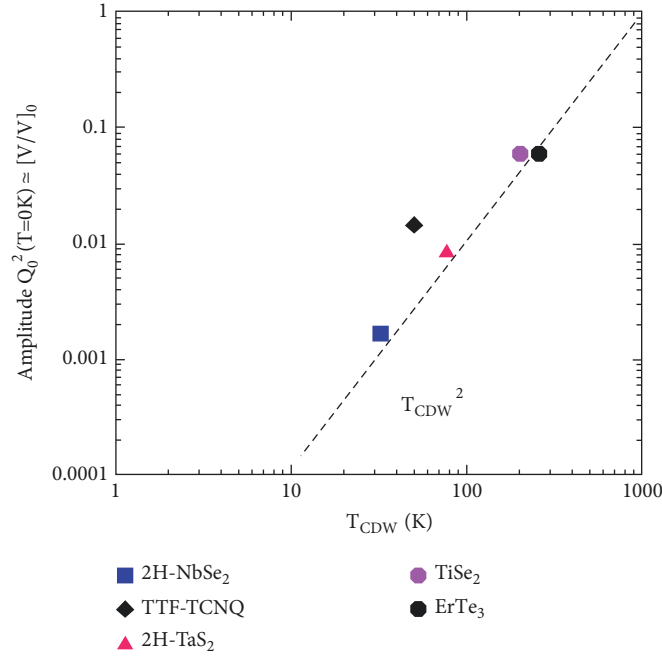
FIGURE 7: *Color on line*. Amplitudes of the square of the order parameter Q_0^2 at T = 0K, which is proportional to the values $[\Delta V/V]_0$ deduced from Figure 6, are reported as a function of T_{CDW}. The solid line increases as T_{CDW}^2.

superlattice reflections and of the intensities of the Raman modes [1, 8, 14].

4. Conclusions

Similar features in the thermodynamic properties at the CDW phase transition T_{CDW} are found in all the CDW materials under review. The amplitude of the specific heat anomaly at the CDW phase transition T_{CDW} is sample dependent but the amplitude increases (roughly) linearly with increasing T_{CDW} in agreement with a second-order phase transition. The (mean field theory) Ehrenfest equations are approximately satisfied by several compounds: the rare earth tritellurides TbTe$_3$, ErTe$_3$ compounds, the transition metal dichalcogenide 2H-NbSe$_2$ compound, and several quasi-one-dimensional conductors. In contrast large inconsistency in the Ehrenfest relationships is found with the transition metal dichalcogenide compounds 2H-TaSe$_2$ and TiSe$_2$. Lattice anharmonicity acting through the stress dependence of the phase transition temperature T_{CDW} in the rare earth tritelluride compounds is larger than that of the transition metal dichalcogenides and quasi-one-dimensional conductors.

It seems that the elastic property in the CDW ordered phase is related to the temperature dependence of the order parameter which follows a BCS behavior. Finally LaAgSb$_2$ has been classified as a 3D CDW system. The Ehrenfest relationships should be verified in this material.

Conflicts of Interest

The authors declare that they have no conflicts of interest.

References

[1] G. Grüner, "Density Waves in Solids," Frontiers in Physics Ed D. Pines (Addison-Wesley) 1994 and Rev. Mod. 60, 1129, 1988.

[2] H. Frölich, Proc. R. Soc. London A223, 296, 1954.

[3] J. W. Brill, "Elastic properties of low dimensional materials," in *Chap. 10 in Handbook of Elastic Properties of Solids (Volume II) Liquids and Gases*, Levy, Bass, and Stern, Eds., Academic Press, 2001.

[4] P. Monceau, "Electronic crystals: An experimental overview," *Advances in Physics*, vol. 61, no. 4, pp. 325–581, 2012.

[5] X. Zhu, J. Guo, J. Zang et al., "Misconceptions associated with the origin of charge density waves," *Advances in Physics*, vol. 2, pp. 325–581, 2017.

[6] X. Zhu, Y. Cao, J. Zhang et al., "Classification of charge density waves based on their nature," *Proceedings of the National Academy of Sciences*, vol. 24, pp. 2367–2371, 2015.

[7] H.-M. Eiter, M. Lavagni, R. Hackl et al., "Alternative route to charge density wave formation in multiband systems," *Proceedings of the National Academy of Sciences*, vol. 110, pp. 64–96, 2013.

[8] N. Ru, C. L. Condron, G. Y. Margulis et al., "Effect of chemical pressure on the charge density wave transition in rare earth tritellurides RTe$_3$," *Physical Review B*, vol. 77, Article ID 035114, 2008.

[9] N. Ru and I. R. Fisher, "Thermodynamic and transport properties of YTe$_3$, LaTe$_3$ and CeTe$_3$," *Physical Review B*, vol. 73, Article ID 033101, 2006.

[10] V. Brouet, W. L. Yang, X. Zhous et al., "Angle-resolved photoemission study of the evolution of band structure and charge density properties in RTe$_3$ (R=Y, La,Ce,Sm, Gd, Tb, and Dy)," *Physical Review B*, vol. 77, Article ID 235104, 2008.

[11] R. G. Moore, V. Brouet, R. He et al., "Fermi surface evolution across multiple charge density wave transition in ErTe$_3$," *Physical Review B*, vol. 81, Article ID 073102, 2010.

[12] R. G. Moore, W. S. Lee, P. S. Kirchman et al., "Ultrafast resonant soft x-ray diffraction dynamics of the charge density wave in TbTe$_3$," *Physical Review B*, vol. 93, Article ID 024304, 2016.

[13] M. Maschek, S. Rosenbranz, R. Heid et al., "Wave-vector-dependent electron-phonon coupling and the charge density wave transition in TbTe$_3$," *Physical Review B*, vol. 91, Article ID 235147, 2015.

[14] N. Lazarevic, Z. V. Popovic, R. Hu et al., "Evidence of coupling between phonons and charge density waves in ErTe$_3$," *Physical Review B*, vol. 83, Article ID 024302, 2011.

[15] D. A. Zocco, J. J. Hamlin, K. Grube et al., "Pressure dependence of the charge density wave and superconducting states in GdTe$_3$," *Physical Review B*, vol. 91, Article ID 205114, 2015.

[16] M. Barmatz, L. R. Testardi, and F. J. Di Salvo, "Elasticity measurements in the layered dichalcogenides TaSe$_2$ and NbSe$_2$," *Physical Review B*, vol. 12, no. 10, pp. 4367–4376, 1975.

[17] M. H. Jericho, A. M. Simpson, and R. F. Frindt, "Velocity of ultrasonic waves in 2H-NbSe$_2$, 2H-TaS$_2$ and 1T-TaS$_2$," *Physical Review B*, vol. 22, no. 10, pp. 4907–4914, 1980.

[18] O. Sezerman, A. M. Simpson, and M. H. Jericho, "Thermal expansion of 1T-TaS$_2$ and 2H-NbSe$_2$," *Solid State Communications*, vol. 36, pp. 737–740, 1980.

[19] V. Eremenko, V. Sirenko, V. Ibulaev, J. Bartolomé, A. Arauzo, and G. Reményi, "Heat capacity, thermal expansion and pressure derivative of critical temperature at the superconducting and charge density wave (CDW) in NbSe$_2$," *Physica*, vol. 469, no. 7-8, pp. 259–264, 2009.

[20] A. Caillé, Y. Lepine, M. H. Jericho et al., "Thermal expansion, ultrasonic velocity, and attenuation measurements in TiS$_2$, TiSe$_2$ and TiS$_{0.5}$Se$_{1.5}$," *Physical Review*, vol. 26, no. 10, p. 5454, 1983.

[21] W. G. Stirling, B. Dorner, J. D. N. Cheeke et al., "Acoustic phonons in the transition metal dichalcogenide layer compound TiSe$_2$," *Solid State Communications*, vol. 18, no. 7, pp. 931–933, 1976.

[22] R. A. Craven, F. J. Di Salvo, F. S. L. Hsu et al., "Mechanisms for the 200 K transition in TiSe$_2$: A measurement of the specific heat," *Solid State Communication*, vol. 25, pp. 39–42, 1978.

[23] J. P. Castellan, S. Rosenkranz, R. Osborn et al., "Chiral phase transition in charge ordered 1T-TiSe$_2$," *Physical Review Letters*, vol. 110, no. 19, Article ID 196404, 2013.

[24] R. A. Craven and S. F. Meyer, "Specific heat and resisitivity near the charge density wave phase transitions in 2H-TaSe$_2$ and 2H-TaS$_2$," *Physical Review B*, vol. 16, no. 10, p. 4583, 1977.

[25] D. Maclean and M. H. Jericho, "Effect of the charge density wave transition on the thermal expansion of 2H-TaSe$_2$, NbSe$_3$ and o-TaS$_3$," *Physical Review B*, vol. 47, no. 24, pp. 16169–16177, 1993.

[26] S. Tomic, K. Biljakovic, D. Djurek et al., "Calorimetric study of the phase transition in Niobium triselenide NbSe$_3$," *Solid State Communications*, vol. 38, pp. 109–112, 1981.

[27] J. W. Brill and N. P. Ong, "Young's modulus of NbSe$_3$," *Solid State Communications*, vol. 25, no. 12, pp. 1075–1078, 1978.

[28] W. L. McMillan, "Microscopic model of charge density waves in 2H-TaSe$_2$," *Physical Review B*, vol. 16, no. 2, pp. 643–650, 1977.

[29] J. A. Aronovitz, P. Goldbart, and G. Mozurkewich, "Elastic singularities at the Peierls transition," *Physical Review Letters*, vol. 64, no. 23, pp. 2799–2802, 1990.

[30] R. S. Kwok, G. Gruner, and S. E. Brown, "Fluctuations and Thermodynamics of the charge density wave phase transition," *Physical Review Letters*, vol. 65, no. 3, pp. 365–368, 1990.

[31] J. W. Brill, M. Chung, Y.-K. Kuo et al., "Thermodynamics of the charge density wave transition in blue bronze," *Physical Review Letters*, vol. 74, no. 7, pp. 1182–1185, 1995.

[32] M. R. Hauser, B. B. Platt, and G. Mozurkewich, "Thermal expansion associated with the charge density wave in K$_{0.3}$MoO$_3$," *Physical Review B*, vol. 43, no. 10, p. 8105, 1991.

[33] L. C. Bourne and A. Zettl, "Elastic anomalies in the charge density wave conductor K$_{0.3}$MoO$_3$," *Solid State Communications*, vol. 60, no. 10, pp. 789–792, 1986.

[34] D. C. Johnston, "Thermodynamics of charge density waves in quasi one dimensional conductors," *Physical Review Letters*, vol. 52, no. 23, p. 2049, 1984.

[35] R. A. Craven, M. B. Salamon, G. DePasquali et al., "Specific heat of Tetrathiofulvalinium-Tetracyanoquinodimethane (TTF-TCNQ) in he vicinity of the metal-insulator transition," *Physical Review Letters*, vol. 32, no. 14, pp. 769–772, 1974.

[36] T. Tiedje, R. R. Haering, M. H. Jericho et al., "Temperature dependence of sound velocities in TTF-TCNQ," *Solid State Communications*, vol. 23, no. 10, pp. 713–718, 1977.

[37] M. Barmatz, L. R. Testardi, A. F. Garito et al., "Elastic properties of one dimensional compounds," *Solid State Communications*, vol. 15, no. 8, pp. 1299–1302, 1974.

[38] D. E. Schafer, G. A. Thomas, and F. Wudl, "High resolution thermal expansion measurements of tetrathiafulvalene-tetracyanoquinodimethane (TTF-TCNQ)," *Physical Review*, vol. 12, no. 12, p. 5532, 1975.

[39] M. Saint-Paul, S. Holtmeier, R. Britel et al., "An ultrasonic and thermal expansion study of the quasi one dimensionbal compound (TaSe$_4$)$_2$I," *Journal of Physics: Condensed Matter*, vol. 8, no. 12, pp. 2021–2041, 1996.

[40] D. Staresinic, A. Kiss, K. Biljakovic et al., "Specific heat of the charge density wave compounds o-TaS$_3$ and (TaSe$_4$)$_2$I," *The European Physical Journal B*, vol. 29, pp. 71–77, 2002.

[41] M. Saint-Paul, C. Guttin, P. Lejay et al., "Elastic anomalies at the charge density wave transition in TbTe$_3$," *Solid State Communications*, vol. 233, pp. 24–29, 2016.

[42] M. Saint-Paul, G. Remenyi, C. Guttin et al., "Thermodynamic and critical properties of the charge density wave system ErTe$_3$," *Physica B*, vol. 504, pp. 39–46, 2017.

[43] M. Saint-Paul, C. Guttin, P. Lejay et al., "Elastic properties of the charge density wave system HoTe$_3$," *Internatiuonal Journal of Modern Physics B*, vol. 32, no. 23, Article ID 1850249, 2018.

[44] S. L. Bud'ko, S. A. Law, P. C. Canfield, and et al, "Thermal expansion and magnetostriction of pure and doped RAgSb$_2$ (R=Y, Sm, La) single crystals," *Journal of Physics: Condensed Matter*, vol. 20, Article ID 115210, 2008.

[45] C. S. Lue, Y. F. Tao, K. M. Sivakumar et al., "Weak charge density wave transition in LaAgSb$_2$ investigated by transport, thermal and NMR studies," *Journal of Physics: Condensed Matter*, vol. 19, no. 40, Article ID 406230, 2007.

[46] K. Rossnagel, "On the origin of charge density waves in select layered transition metal dichalcogenides," *Journal of Physics: Condensed Matter*, vol. 23, Article ID 213001, 2011.

[47] L. Landau and E. Lifshitz, *Statistical Physics*, Pergamon Press, 1968.

[48] L. R. Testardi, "Elastic modulus, thermal expansion, and specific heat at a phase transition," *Physical Review B*, vol. 12, no. 9, pp. 3849–3854, 1975.

[49] R. A. Cowley, "Structural phase transitions," *Advances in Physics*, vol. 39, no. 1, pp. 1–110, 1980.

[50] R. Blink and A. P. Levanyk, *Incommensurate Phases in Dielectrics: Fundamentals vol. 1 modern Problems in Condensed Matter Sciences*, Elsevier Ltd, 1986.

[51] W. Rehwald, A. Vonlanthen, J. K. Krüger et al., "Study of the elastic properties of K_2SeO_4 at the phase transition to incommensurate and the commensurate phase by ultrasonic techniques and Brillouin spectroscopy," *Journal of Physics C: Solid State Physics*, vol. 13, no. 20, pp. 3823–3834, 1980.

[52] W. Rehwald, "The study of structural phase transitions by means of ultrasonic experiments," *Advances in Physics*, vol. 22, pp. 721–755, 1973, B. Luthi, "Physical Acoustic in the solid state" Springer-Verlag Berlin 2005.

[53] R. Weber and R. Street, "The heat capacity anomaly of chromium at 311 K (antiferromagnetic to paramagnetic transition)," *Journal of Physics F: Metal Physics*, vol. 2, no. 5, pp. 873–877, 1972.

[54] D. I. Bolef and J. De Klerk, "Anomalies in the elastic constants and thermal expansion of chromium single crystals," *Physical Review*, vol. 129, no. 3, pp. 1063–1067, 1963.

[55] M. B. Walker, "Phenomenological theory of the spin density wave state of chromium," *Physical Review*, vol. 22, no. 3, p. 1338, 1980.